Neoplasia 49 (2024) 100973

Contents lists available at ScienceDirect

Neoplasia

journal homepage: www.elsevier.com/locate/neo

FBXO38 deficiency promotes lysosome-dependent STING degradation and inhibits cGAS–STING pathway activation

Yijia Wu [a,b], Yao Lin [c], Feiyang Shen [a,b], Rui Huang [a,b], Zhe Zhang [a,b,c], Min Zhou [a,b], Yan Fang [a,b,*], Jianfeng Shen [a,b,c,*], Xianqun Fan [a,b,*]

[a] Department of Ophthalmology, Ninth People's Hospital, Shanghai Jiao Tong University School of Medicine, Shanghai 200025, China
[b] Shanghai Key Laboratory of Orbital Diseases and Ocular Oncology, Shanghai 200025, China
[c] Institute of Translational Medicine, National Facility for Translational Medicine, Shanghai Jiao Tong University, Shanghai 200240, China

ARTICLE INFO

Keywords:
FBXO38
STING
IFNA1
CCL5
cGAS–STING pathway

ABSTRACT

F-box only protein 38 (FBXO38) is a member of the F-box family that mediates the ubiquitination and proteasome degradation of programmed death 1 (PD-1), and thus has important effects on T cell-related immunity. While its powerful role in adaptive immunity has attracted much attention, its regulatory roles in innate immune pathways remain unknown. The cyclic GMP–AMP synthase–stimulator of interferon genes (cGAS–STING) pathway is an important innate immune pathway that regulates type I interferons. STING protein is the core component of this pathway. In this study, we identified that FBXO38 deficiency enhanced tumor proliferation and reduced tumor $CD8^+$ T cells infiltration. Loss of FBXO38 resulted in reduced STING protein levels *in vitro* and *in vivo*, further leading to preventing cGAS–STING pathway activation, and decreased downstream product IFNA1 and CCL5. The mechanism of reduced STING protein was associated with lysosome-mediated degradation rather than proteasomal function. Our results demonstrate a critical role for FBXO38 in the cGAS–STING pathway.

Introduction

Therapeutic antibodies targeting the programmed death 1 (PD-1)/programmed death-ligand 1 (PD-L1) pathway have been applied to many cancers including melanoma, colon cancer, cervical cancer, and kidney cancer [1,2]. However, these therapies are greatly limited by immune checkpoint blockade.

The cyclic GMP–AMP synthase–stimulator of interferon genes (cGAS–STING) pathway is a classical DNA damage response pathway that is characterized by activation of interferon regulatory factor 3 (IRF3) and expression of type I interferons (IFNs; e.g. IFN-α/β) [3,4]. The combination of targeting PD-1 and the cGAS–STING pathway inhibitions has been proven to effectively activate $CD8^+$ T cells in the tumor immune microenvironment and further enhance anti-tumor efficacy [5,6]. Following stimulation by aberrant DNA accumulation or pathogenic infection [7], cGAS promotes a conformational change in STING protein [8], allowing it to translocate to the Golgi apparatus [9]. Here, STING dimerizes and recruits tank-binding kinase 1 (TBK1), which phosphorylates the transcription factor IRF3 [10], ultimately leading to the expression of type I IFNs and downstream chemokine secretion including of CCL5, CXCL9, and CXCL10 [11,12] to recruit $CD8^+$ T cells. Components of the cGAS–STING pathway are regulated by multiple posttranslational modifications (PTMs) and highly depend on the regulation of vesicle trafficking [13]. The common PTMs of STING include phosphorylation, ubiquitination, and palmitoylation [14]. The activation of STING can also be suppressed by blocking the transport of STING from the endoplasmic reticulum (ER) to the perinuclear compartments [15] or from the ER-Golgi intermediate compartment to Golgi apparatus [16]. After pathway activation, STING itself can be also degraded by autophagy or lysosomal function [13,17].

Abbreviations: c-Cbl, casitas B lymphoma; cGAS–STING pathway, cyclic GMP–AMP synthase–stimulator of interferon genes pathway; DCs, mature dendritic cells; DEGs, differentially expressed genes; DUBs, deubiquitinases; FBXO38, F-box only protein 38; GO, Gene Ontology; GSEA, Gene set enrichment analysis; IFNs, type I interferons; IRF3, interferon regulatory factor 3; KEGG, Kyoto Encyclopedia of Genes and Genomes; KLF7, Kruppel-like factor 7; LAMP1, lysosomal-associated membrane protein 1; OS, overall survival; PD-1, programmed death 1; PD-L1, programmed death-ligand 1; PTMs, posttranslational modifications; RNA-seq, RNA-sequencing; SCF, SKP1-CUL1-F-box protein; TBK1, tank-binding kinase 1.

* Corresponding authors.
E-mail addresses: yanyan2021fang@sjtu.edu.cn (Y. Fang), jfshen@shsmu.edu.cn (J. Shen), fanxq@sjtu.edu.cn (X. Fan).

https://doi.org/10.1016/j.neo.2024.100973
Received 19 January 2023; Received in revised form 11 January 2024; Accepted 18 January 2024

Elucidating potential mechanisms of PD-1/PD-L1 regulation is another focus of improving the efficiency of treatment. PD-1/PD-L1 expression can be modulated by several processes including transcription, posttranscriptional modifications, and PTMs [18]. A previous study uncovered that F-box only protein 38 (FBXO38) mediates Lys48-linked poly-ubiquitination and subsequent proteasomal degradation of PD-1 in activated T cells [19]. In an animal model, FBXO38 deficiency in T cells worsened anti-tumor efficacy and promoted tumor growth. Together, these findings suggest that FBXO38 contributes to cancer immunotherapy by regulating PD-1. FBXO38, which belongs to the SKP1-CUL1-F-box protein (SCF) family, was initially discovered as a coactivator of the Kruppel-like factor 7 (KLF7) transcription factor, which participates in neuronal axon outgrowth and repair [20]. Previous studies have focused on FBXO38's function in centromere integrity, sertoli cell maturation, and distal spinal muscular atrophy [21–23]. However, how FBXO38 acts on innate immune pathways in tumors is unknown.

To explore the possibility of improving anti-PD-1/PD-L1 therapy by combining these agents with DNA damage response inhibitors targeting FBXO38, we investigated the potential roles of FBXO38 in the cGAS–STING pathway. In this study, we constructed FBXO38-knockdown cell lines and uncovered the resultant phenotypes in tumors. We demonstrated that FBXO38 deficiency led to increased tumor proliferation, greater lysosomal degradation of STING protein, inhibited cGAS–STING pathway activation and decreased secretion of the downstream IFNA1 and CCL5. This phenotype was also confirmed in animal models. These findings reveal that FBXO38 plays an important role in the cGAS–STING pathway. Considering that FBXO38 can mediate PD-1 degradation in T cells, it may open a new venue for restoring susceptibility to anti-PD1/PD-L1 therapy.

Materials and methods

Cell culture and transfection of plasmids

HEK293FT, HCT116, HeLa, 92.1, and B16F10 cells were purchased from the Cell bank of the Chinese Academy of Science. All cell lines tested negative for mycoplasma contamination. B16F10, HCT116 and HEK293FT cells were cultured in Dulbecco's modified Eagle's medium (DMEM; Gibco, Waltham, MA, USA) supplemented with 10 % certified heat-inactivated fetal bovine serum (FBS; Gibco), penicillin (100 U/mL), and streptomycin (100 μg/mL) at 37°C in a humidified 5 % CO_2 atmosphere. HeLa and 92.1 cells were cultured in RPMI 1640 medium containing 10 % FBS. For knockdown of FBXO38 and STING and overexpression of FBXO38, HEK293FT cells were transfected with packaging plasmids (psPAX2 and PMD.2G, purchased from Addgene) combined with PLKO.1-based vectors (knockdown) or PLVX-based vectors (overexpression) using Polyjet In Vitro DNA Transfection Reagent (SignaGen, Germany) in accordance with the manufacturer's instructions. Forty-eight hours after transfection, virus-containing supernatants were collected, combined with Polybrene (Solarbio), and used to culture tumor cells for 24 h. Knockdown and overexpression efficiencies were identified by immunoblot. The shRNA sequences were as follows: human FBXO38: 5′-GACTTCCTTTGTATCAGCTTA-3′ and 5′-GCAAGACTCCACTTCGAAAGA-3′; mouse fbxo38: 5′-GCATTTAGTTGGTGTCAATGT-3′ and 5′-GCCATGAAACGAAAGCGAA-3′; human STING: 5′-GCTGTATATTCTCCTCCCATT-3′ and 5′-GCATGGTCATATTACATCGGA-3′. To get FBXO38-overexpression plasmids, the homologous cDNA sequence for FBXO38-Flag was cloned into the vector. All constructs were confirmed by sequencing.

qPCR

Total RNA was extracted from cells with the EZ-press RNA Purification Kit (B0004D, EZBioscience). Animal tissues were lysed using stainless steel beads (5 mm) in a Tissuelyser-48L (Shanghai Jingxin), and then extracted with TRIzol in accordance with the manufacturer's instructions (Life Technologies). Reverse transcription of cDNA was performed using the 4 × Reverse Transcription Master Mix (A0010GQ, EZBioscience). cDNA was subjected to qPCR using a Real-Time PCR System (Applied Biosystems). The primers used included human CCL5_forward: 5′-CGTGCCCACATCAAGGAGTA-3′; human CCL5_reverse: 5′-TCGGGTGACAAAGACGACTG-3′; mouse ccl5_forward: 5′-TGCTGCTTTGCCTACCTCTC-3′; mouse ccl5_reverse: 5′-TCCTTCGAGTGACAAACACGA-3′; human STING_forward: 5′-CACTTGGATGCTTGCCCTC-3′; human STING_reverse: 5′-GCCACGTTGAAATTCCCTTTTT-3′; mouse sting_forward: 5′-GCTGCTGTCTCCCCATTCAG-3′; mouse sting_reverse: 5′-GCTGGATGCAGGTTGGAGTA-3′; human FBXO38_forward: 5′-AACGGTACTCGGCGTTACTC-3′; human FBXO38_reverse: 5′-TGTTTTGGCTACTTCTGACAATTC-3′; mouse fbxo38_forward: 5′-CTCCAAGAAGTCTGGGCTCC-3′; and mouse fbxo38_reverse: 5′-TTACTGCCGTTTCCCTGGAC-3′; human IFNA1_forward: TCAAAGACTCTCACCCCTGC; human IFNA1_reverse: CAGTGTAAAGGTGCACATGACG; mouse IFNA1_forward: CTACTGGCCAACCTGCTCTC; mouse IFNA1_reverse: CTGCGGGAATCCAAAGTCCT.

Western blotting and immunoprecipitation

Cells and animal tissues were lysed in RIPA buffer (50 mM Tris-HCl [pH 7.4], 150 mM NaCl, 1 % NP-40, 0.1 % SDS, 0.5 % sodium deoxycholate, 2 mM Na3VO4, 20 mM NaF, 1 mM PMSF, 100 × protease inhibitor Cocktail [Sangon, C600387-0001], and 1 × phosphatase inhibitor complex I [Sangon, C500017-0001]). Following the addition of 5 × SDS loading buffer, samples were heated for 5 min at 95°C. Next, proteins were separated by 8 %–12 % SDS-PAGE. Following electrophoretic transfer of proteins onto PVDF membranes (Millipore, GVWP14250 or HVLP14250), non-specific binding was blocked by incubation with 5 % skim milk. Membranes were incubated with the following primary antibodies: anti-FBXO38 (BETHYL, A302-378A, 1:2000), anti-STING (CST, D2P2F, 1:1000), anti-p-STING (CST, E9A9K, 1:1000), anti-TBK1 (CST, E8I3G, 1:1000), anti-p-TBK1 (CST, D52C2, 1:1000), anti-IRF3 (CST, D6I4C, 1:1000), anti-p-IRF3 (ABclonal, AP0857, 1:1000), and anti-β-actin (ABclonal, A17910, 1:10000). Membranes were then washed and incubated with a fluorescent secondary antibody of the corresponding species for 1 h including: Alexa Fluor™ Plus 800 goat anti-mouse IgG (H+L) (Invitrogen, A32730, 1:10000), StarBright Blue 520 goat anti-mouse IgG (Bio-Rad, 12005867, 1:10000), and Alexa Fluor™ Plus 800 goat anti-rabbit IgG (H+L) (Invitrogen, A32735, 1:10000). Immunoreactive bands were visualized using the ChemiDoc™ MP Imaging System (#12003154) and analyzed with ImageJ (v1.53t)

STING and lysosome colocalization analysis

Cells were incubated on cover glass at a density of 20 % to 30 % and cultured in the appropriate medium at 37°C for 24 h. After incubation, cells were fixed in 4 % paraformaldehyde for 10 min and permeabilized with PBS containing 0.5 % Triton X-100 for 3 min. Cells were then incubated in PBS containing 1 % skim milk for 1 h. The two primary antibodies were incubated together at 4°C for 24 h, and the two secondary antibodies were incubated at room temperature in the dark for 1 h. The antibodies used included: rabbit anti-STING mAb (CST, E9X7F, 1:1000), mouse anti-LAMP1 mAb (CST, D4O1S, 1:100), anti-rabbit IgG (H+L), F(ab')2 Fragment (Alexa Fluor® 488 Conjugate) (CST, #4412, 1:2000), anti-mouse IgG (H+L), F(ab')2 Fragment (Alexa Fluor® 555 Conjugate) (CST, #4409, 1:2000). Finally, the cells were stained with DAPI (Beyotime, C1002) for 30 min at room temperature, and the coverslips were mounted with anti-fade mounting medium (Beyotime, P0126). Images were acquired by confocal laser scanning microscopy (Leica TCS SP8 STED 3X_) using a 63 × 1.4 NA oil-immersion objective.

Mouse xenograft tumor model

C57BL/6 and BALB/c nude mice were purchased from Charles River laboratory, and 6- to 8-week-old male mice were divided by the blinded method for use in experiments. All experiments were approved by the Institutional Animal Care and Use Committee (IACUC) of Shanghai Jiao Tong University Laboratory Animal Center and were performed in accordance with relevant experimental guidelines.

Briefly, 1×10^6 B16F10 and 3×10^6 HCT116 cells were subcutaneously injected into the flank of each mice. Tumor sizes were measured in two dimensions by digital calipers every 2 d. Tumor volumes were calculated according to the formula: $V = (L \times l^2)/2$, where L = widest and l = smallest diameter. When the maximum tumor volume reached 2000 mm^3, the mice were sacrificed by cervical dislocation. Tumors were dissected and separated for weighing. Tumor tissues were divided into three parts for subsequent experiments, including sectioning and staining, western blotting, and qPCR.

Immunohistochemistry

Immunohistochemical sections and staining were done by the Servicebio laboratory. To stain xenograft tumor tissues, samples were first fixed in 4 % paraformaldehyde and then sent to Servicebio. The experiments were based on standard protocols. For immunostaining of tissue sections, slides were progressively dewaxed in xylene, and then rehydrated and boiled for 20 min in citrate buffer (10 mM, pH 6.0) for antigen retrieval. Subsequently, slides were blocked in PBST with 3 % BSA for 30 min at room temperature and incubated with anti-STING primary antibody (CST, D2P2F, 1:1000) in PBST at 4°C overnight. Sections were incubated with secondary antibody at room temperature for 1 h. Then, slides were stained with DAPI for 30 min at room temperature and coverslipped with anti-fade mounting medium (Beyotime, P0126). Fluorescent images were obtained by Panoramic MIDI.

Flow cytometry (FCM)

FCM panels were used to assess percentages of mature dendritic cells (DCs) and $CD8^+$ T cells. For these panels, the following monoclonal antibody conjugates were used: CD80 (biolegend, 105021), CD86 (biolegend, 104713), CD45 (biolegend, 103128), CD11c (biolegend, 117306), CD3 (biolegend, 100206), CD4 (biolegend, 100528), CD8 (biolegend, 100712). For stainings, 100μL of single-cell suspensions was incubated with antibodies for 15 min at room temperature, followed by PBS washing and resuspended. FCM data acquisition was performed on flow cytometer (Beckman, CytoFLEX). Analysis was performed on FlowJo software (Ashland, Oregon, USA).

RNA sequencing (RNA-seq), library generation, and bioinformatics analysis

RNA was isolated with the EZ-press RNA Purification Kit (B0004D, EZBioscience) and submitted to the Personalbio Laboratory for stranded library preparation. In total 1 μg of RNA per sample was used for RNA sample preparation. Sequencing libraries were generated using the NEBNext® UltraTM RNA Library Prep Kit for Illumina® (NEB, USA), and the quality was assessed on the Agilent Bioanalyzer 2100 system. After cluster generation, the library preparations were sequenced on an Illumina Novaseq 6000 platform, and 150 bp paired-end reads were generated. Sequences were aligned to the human or mouse genome using Hisat2 v2.0.5. Differential expression analysis was performed by the DESeq2 R package (1.16.1). Next, Gene Ontology (GO) and Kyoto Encyclopedia of Genes and Genomes (KEGG) pathways enrichment analysis of DEGs was implemented by the clusterProfiler R package. Gene set enrichment analysis (GSEA) was performed using default settings. Tumor microenvironment was calculated by CIBERSORT website (https://cibersortx.stanford.edu/). All sequencing data have been uploaded to the Gene Expression Omnibus database under the accession number GSE220879 and GSE246258.

Statistical analysis

All data were acquired from at least three independent biological replicates and are reported as mean±SEM. Data were analyzed by unpaired and two-tailed Student's t-tests using GraphPad Prism 8 software (GraphPad Software, Inc., San Diego, CA, USA). All analyses were carried out on normally distributed data; ns, not significant; *$p<0.05$; **$p<0.01$; ***$p<0.001$.

Results

FBXO38 deficiency stimulated tumor growth in vivo

To reveal the role of FBXO38 in tumor proliferation, we first investigated the GEPIA database (http://gepia.cancer-pku.cn/) [24]. FBXO38 was universally expressed in 30 tumor and normal tissues from The Cancer Genome Atlas (**Supplement fig. 1A**). We selected several cells to validate FBXO38 protein levels by Western blotting (Fig. 1**A**). According to the actual FBXO38 expression, we constructed FBXO38-knockdown cell lines in B16F10 (mouse melanoma cells), HCT116 (human colorectal cancer cells), HeLa (human cervical cancer cells), and 92.1 (human uveal melanoma cells) by shRNA. As shown in Fig. 1**B** and **Supplement fig. 1C-E**, immunoblotting showed that the efficiency of knockdown was greater than 80 %.

To identify whether FBXO38 mediated tumor growth in the absence of immune environment *in vivo*, we constructed HCT116-bearing BALB/c nude mice by subcutaneous injection of HCT116 cells. We observed changes in tumor volumes and excised tumors to record tumor weights on day 21 (**Supplement fig. 1F**). Compared with the control group, tumor volumes were significantly increased in the shFBXO38 #1 ($p=0.0201$) and shFBXO38 #2 ($p=0.0173$) groups (**Supplement fig. 1G**). Mean tumor weights in the shFBXO38 #1 and shFBXO38 #2 groups were 5.5- and 3.3-fold higher compared with the control group, respectively (**Supplement fig. 1H**). Resected tumors were assayed for proliferative activity with Ki-67 staining. We observed that there was 1.21- to 1.39-fold increased expression of Ki-67 in the two FBXO38-knockdown groups (**Supplement fig. 1I-J**).

Clinically, low FBXO38 expression was associated with poor overall survival (OS) in skin cutaneous melanoma ($p=0.034$, **Supplement fig. 1B**). To identify whether FBXO38 affected tumor growth *in vivo* by regulating immune environment, we constructed B16F10-bearing C57BL/6 mice by subcutaneous injection of B16F10 cells (Fig. 1**C**). In comparison with the control group, tumor volumes significantly increased in the shFBXO38 #1 ($p<0.001$) and shFBXO38 #2 ($p<0.0001$) groups on day 16 (Fig. 1**D**). Tumor weights in the shFBXO38 #1 ($p=0.004$) and shFBXO38 #2 ($p=0.023$) groups were also significantly increased compared with the control group, respectively (Fig. 1**E**).

Altogether, *in vivo* experiments suggested that loss of FBXO38 activated tumor growth with or without immune environment. However, how FBXO38 regulates tumor proliferation remained unknown.

FBXO38 altered $CD8^+$ T cells infiltration in vivo through the interferon alpha response pathway

To investigate possible mechanisms through which FBXO38 influenced tumor growth, we first employed transcriptional profiling of tumor cells *in vitro* with or without FBXO38 knockdown. RNA-seq of HCT116 and HeLa cells was performed. Differentially expressed genes (DEGs) were selected according to P-value ≤ 0.05 and fold change ≥ 2. The distribution of DEGs was exhibited by the volcano plot in **Supplement fig. 2A**, and hierarchical clustering in a heatmap was shown in **Supplement fig. 2B**. There were 947 DEGs, including 383 upregulated

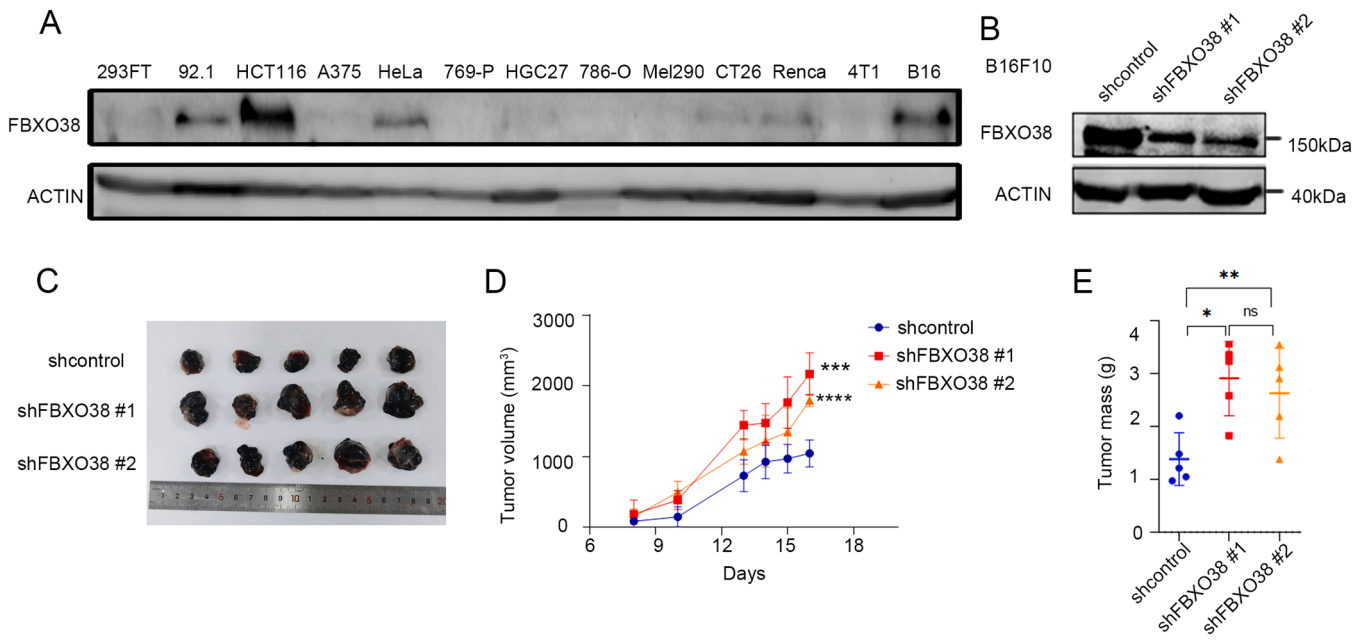

Fig. 1. FBXO38 deficiency promoted tumor growth *in vivo*. A. Immunoblot assays are shown to validate FBXO38 protein levels in different cells. B. Immunoblot assays are shown to validate changes in FBXO38 protein levels in FBXO38 knockdown cells. C. C57BL/6 mice were subcutaneously injected with 1×10^6 B16F10 cells. Tumor volumes were then monitored for 16 d. Mice and excised tumors from the three representative groups displayed for imaging. D. Tumor growth curves. Data are representative of two independent experiments (n=5). Data are presented as mean±SEM and were analyzed by two-tailed unpaired Student's t-test; ***p<0.001. E. Tumor weights in the three groups. Each symbol represents one mouse. Data are pooled from two independent experiments. Data are mean±SEM; *p<0.05, **p<0.01, (two-tailed t-test); ns, not significant.

and 564 downregulated genes. It is worth noting that the expression of IFNA1 was significantly decreased in the FBXO38 knockdown group (p=0.016, **Supplement fig. 2A**). Next, we enriched the DEGs by GO (**Supplement fig. 2C**) and KEGG analysis (**Supplement fig. 2D**). DEGs were primarily involved in nature killer cell mediated cytotoxicity, antigen processing and presentation and T cell receptor signaling pathway. According to GSEA (**Supplement fig. 2E-F**), FBXO38 was positively correlated with T cell receptor signaling pathway and Fc gamma R-mediated phagocytosis, and negatively correlated with complement and coagulation cascades. It implied that FBXO38 may interact with the immune pathway in the tumor.

To identify how FBXO38 regulated tumor growth in immune environment *in vivo*, RNA-sequencing was also performed on resected B16F10 tumors. Volcano plot revealed the distribution of DEGs, which were chosen according to P-value ≤0.05 and fold change ≥2 (Fig. 2**A**). There were 300 DEGs, including 20 upregulated and 280 downregulated genes. KEGG analysis suggested that DEGs was associated with Th1 and Th2 cell differentiation (Fig. 2**B**). GSEA uncovered that the control group was positively correlated with interferon alpha response pathway (Fig. 2**C**).

It is reported that IFN-α increased the infiltration of $CD8^+$ T cells into microenvironment [25]. To investigate changes in $CD8^+$ T cells in tumor microenvironment, CIBERSORT analysis and FCM were utilized. CIBERSORT revealed decreased $CD8^+$ T cells in shFBXO38 groups (Fig. 2**D**). According to FCM, percentage of both mature DCs (p<0.0001 and p<0.0001, respectively, Fig. 2**E**) and $CD8^+$ T cells (p=0.017 and p=0.001, respectively, Fig. 2**F**) were significantly reduced in lymph gland. In spleen tissue, both mature DCs (p<0.001 and p<0.001, respectively, Fig. 2**G**) and CD8+ T cells (p<0.0001 and p<0.0001, respectively, Fig. 2**H**) were significantly decreased. It implied that FBXO38 deficiency blocked $CD8^+$ T cells infiltration *in vivo* through the interferon alpha response pathway.

FBXO38 mediated STING degradation

Considering the downregulation of IFN-α in the FBXO38-knockdown group, we focused subsequent experiments on the cGAS–STING pathway, a classic innate immune pathway. To explore the possible mechanism through which FBXO38 regulates innate immunity, we checked protein and transcription levels of each component of the cGAS–STING pathway in B16F10, HCT116, HeLa, and 92.1 FBXO38-knockdown cell lines. With decreased FBXO38 expression, STING protein was reduced in B16F10 (Fig. 3**A**), HCT116 (Fig. 3**B**), 92.1 (Fig. 3**C**), and HeLa (Fig. 3**D**) cells; meanwhile, STING's transcriptional level was unchanged (Fig. 3**E-H**). Therefore, we speculated that FBXO38 only affected STING expression at the protein level. We next overexpressed FBXO38 in B16F10 and HCT116 cells. As shown in Fig. 3**I** and Fig. 3**J**, STING expression was increased in the FBXO38-overexpression B16F10 and HCT116 cells. To demonstrate whether STING has a similar effect on FBXO38, we constructed STING-knockdown HCT116 cell lines, and FBXO38 protein levels remained the same (Fig. 3**K**). *In vivo*, STING protein levels were measured by immunohistochemistry and western blotting. STING protein in both B16F10 (Fig. 3**L**) and HCT116 (Fig. 3**M**) FBXO38-knockdown tumor tissues were decreased compared with control tissue. As shown in Fig. 3**N-O**, STING staining was reduced to 0.65- to 0.76-fold in the FBXO38 knockdown HCT116 groups. These results indicated that STING protein levels were positively correlated with FBXO38.

To analyze whether this effect was caused by a direct interaction, we performed co-immunoprecipitation of STING and FBXO38 proteins in HCT116 cells and found no evidence of a direct interaction between the two proteins (**Supplement fig. 3A**).

FBXO38 deficiency inhibits the cGAS-STING pathway

The activation of the cGAS–STING pathway is mainly through phosphorylation of TBK1 and IRF3, and finally stimulates the secretion of downstream IFNA, CCL5, and so on. To identify changes in

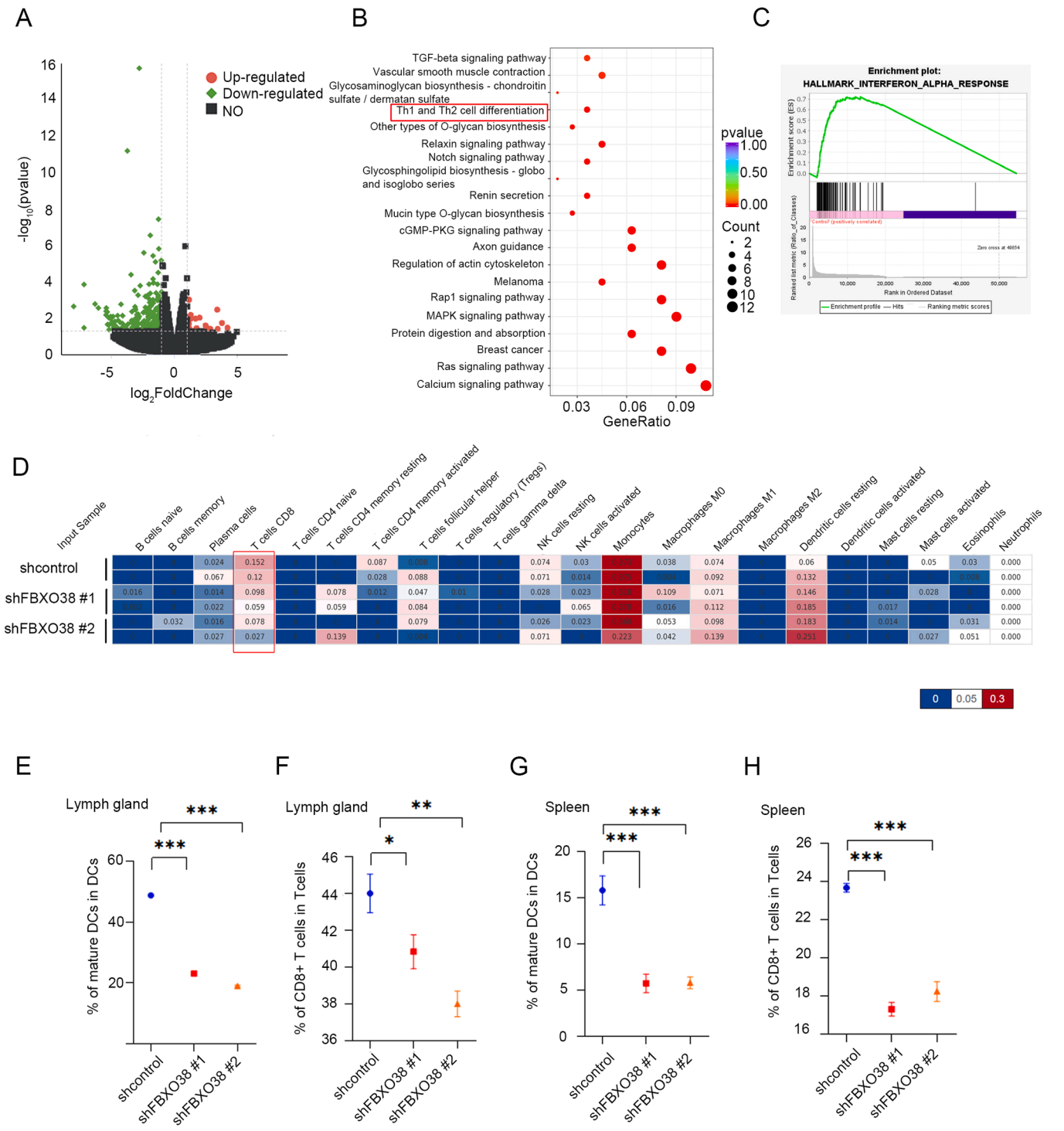

Fig. 2. FBXO38 altered T cell differentiation *in vivo* through the interferon alpha response pathway. A. Visualization of differentially expressed genes (DEGs) between the control and knockdown B16F10 tumor tissue groups by RNA sequencing. Volcano plot representing significant (p-value ≤0.05) and remarkable (|fold-change| ≥2) genes. Red dots represent 20 upregulated genes and green dots represent 280 downregulated genes. B. Dot plots of the top 20 ranked Kyoto Encyclopedia of Genes and Genomes (KEGG) terms of D. Colors of the dots represent P-values, and their sizes represent the number of genes in the list. C. Gene set enrichment analysis (GSEA) depicts the enrichment of the 'interferon alpha response' signature in control compared with FBXO38-knockdown B16F10 tumor tissue groups. D. Estimated proportions of immune cell subsets by Cibersort webserver. The results used a custom RNA-Seq leukocyte signature matrix ('LM6', section 3.3.3). E-H. Flow cytometry (FCM) analysis shows changes in percentages of mature dendritic cells (DCs) and CD8+T cell subsets in lymph gland and spleen. E and F represent DCs and CD8+T cells in lymph gland, respectively, while G and H represent DCs and CD8+T cells in spleen respectively.

downstream components of the cGAS–STING pathway, we examined the protein levels of FBXO38, p-STING, p-TBK1, TBK1, p-IRF3 and IRF3 protein levels in FBXO38 knockdown cells. As is shown in Fig. 4**A-D**, p-STING, p-TBK1, and p-IRF3 were reduced in FBXO38-knockdown groups, while TBK1 and IRF3 stayed the same. We also checked the transcription levels of IFNA1, CCL5, CXCL9, and CXCL10 by real-time quantitative PCR (qPCR). CCL5 and IFNA1 expression was significantly reduced ($p<0.05$) in B16F10 (Fig. 4**E**), HCT116 (Fig. 4**F**), 92.1

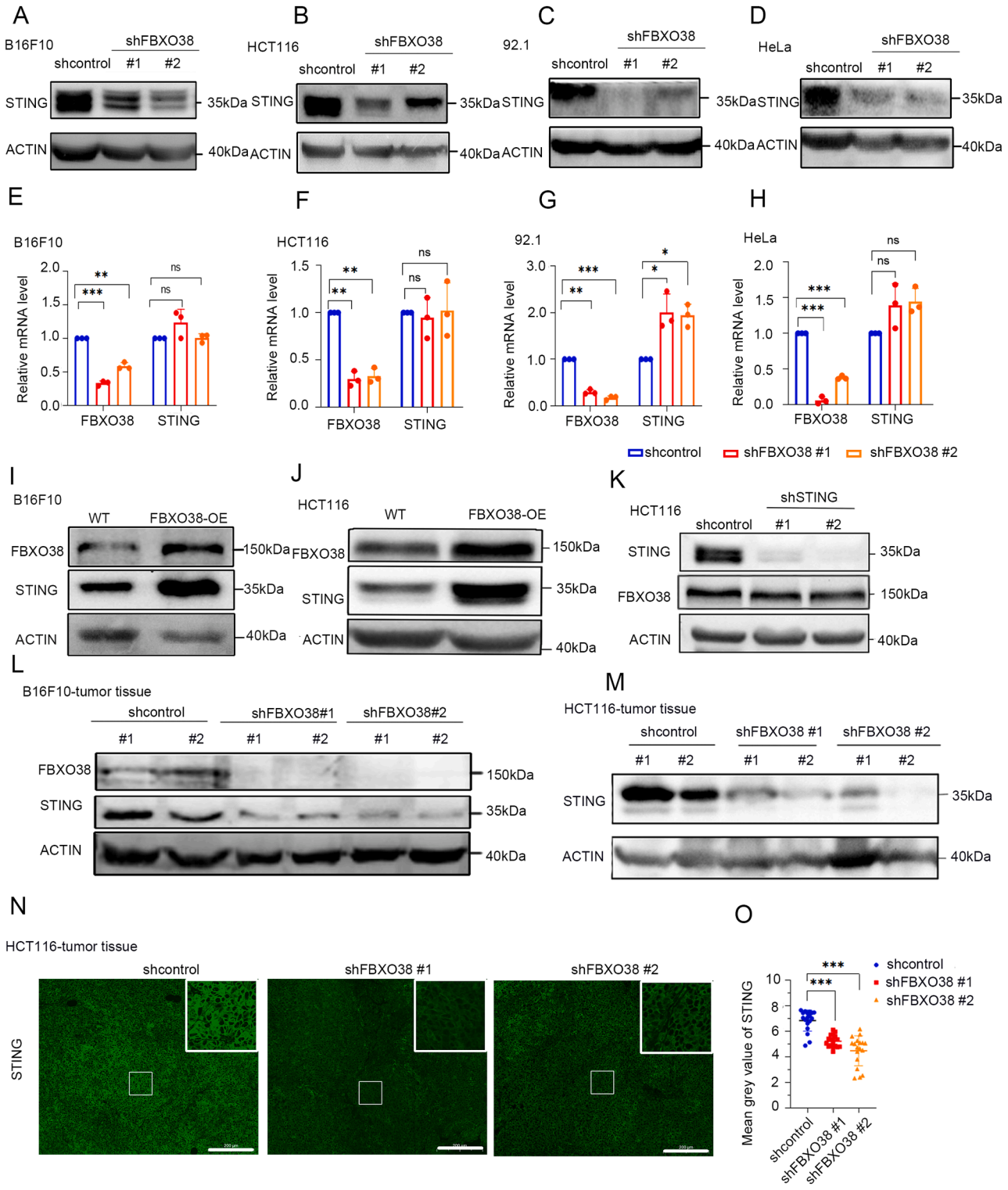

Fig. 3. FBXO38 mediated STING degradation. A-D. Immunoblot assays are shown to validate changes in STING protein levels in FBXO38 knockdown cells. The four images represent changes in B16F10, HCT116, 92.1, and HeLa cells, respectively. E–H. Relative expression levels of FBXO38 and STING as determined by qPCR in different cell lines (n=3). The images represent changes in B16F10, HCT116, 92.1, and HeLa cells, respectively. Graphs are presented as mean±SD; ns, not significant; *p<0.05; **p<0.01; ***p<0.001. I-J. Immunoblotting was used to test FBXO38 and STING protein expression in FBXO38-overexpressing B16F10 (I) and HCT116 cells (J). K. Immunoblot assays are shown to validate changes in STING and FBXO38 protein levels in STING knockdown HCT116 cells. L-M. Immunoblot for FBXO38 and STING protein expression in B16F10 (L) and HCT116 xenograft tumors (M) (n=2). N. Representative data of immunofluorescence staining in the three groups. Tumor tissues were stained with STING (green); scale bars: 200 μm. O. Quantitative analysis of the STING immunofluorescence signal. For graphical presentation, mean gray values were calculated for each group from three slices with six random view fields at 20 × from each slice. Data are presented as mean gray values of STING±SEM; ***p<0.0001.

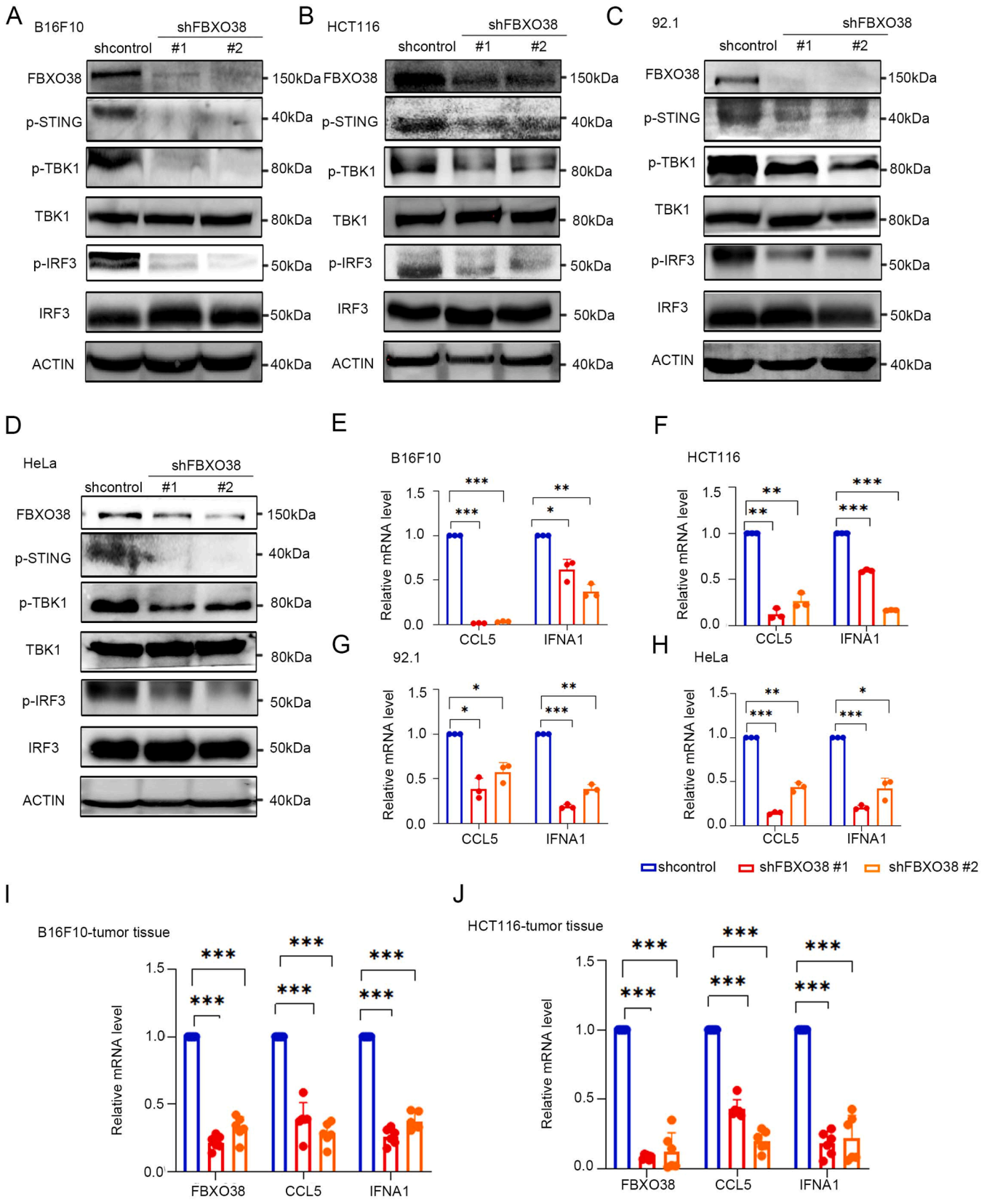

Fig. 4. FBXO38 deficiency inhibits the cGAS-STING pathway. A-D. Immunoblot assays are shown to validate changes in FBXO38, p-STING, p-TBK1, TBK1, p-IRF3 and IRF3 protein levels in FBXO38 knockdown cells. The four images represent changes in B16F10, HCT116, 92.1, and HeLa cells, respectively. E–H. Relative expression levels of CCL5 and IFNA1 as determined by qPCR in different cell lines (n=3). The images represent changes in B16F10, HCT116, 92.1, and HeLa cells, respectively. Graphs are presented as mean±SD; *p<0.05; **p<0.01; ***p<0.001. I-J. Relative FBXO38, CCL5 and IFNA1 expression levels in B16F10 (I) and HCT116 (J) xenograft tumors by three measurements in two tumors from each group; graphs are presented as mean±SD. Graphs are presented as mean ±SD; ***p<0.001.

(Fig. 4**G**), and HeLa (Fig. 4**H**) FBXO38-knockdown cells. CXCL9 or CXCL10 also significantly decreased in B16F10 knockdown group ($p<0.05$) (**Supplement fig. 3E**). However, there were no changes in HCT116, 92.1, and HeLa cells (**Supplement fig. 3F-H**). *In vivo*, relative CCL5 expression was calculated by qPCR. In B16F10 and HCT116 FBXO38-knockdown tumor tissue, CCL5 expression decreased by 2- to 3-fold compared by control groups (Fig. 4**I-J**). These results uncovered that FBXO38 deficiency inhibits cGAS-STING pathway.

To verify that FBXO38 altered CCL5 secretion and tumor growth by regulating STING protein, FBXO38 was overexpressed in the STING-knockdown cells. Additionally, changes in CCL5 secretion (**Supplement fig. 3B**) and clonogenicity (**Supplement fig. 3C-D**) following FBXO38 overexpression disappeared in STING-knockdown cells. Therefore, we hypothesized that FBXO38 affected CCL5 secretion and tumor growth by regulating STING protein levels.

FBXO38 mediated lysosome-depended STING degradation

There are two main mechanisms of STING degradation: proteasomal degradation [14,26] and lysosomal degradation [13]. Therefore, to clarify which pathway was responsible for the STING degradation induced by FBXO38, we pretreated FBXO38-knockdown cell lines with known inhibitors at various concentration, and measured degradation by immunoblot. In both B16F10 and HCT116 cell lines, we detected that STING expression was restored by the lysosomal inhibitors chloroquine (Fig. 5**A and Supplement fig. 4C**) and NH_4Cl (**Supplement fig. 4D**), but not by the proteasome inhibitor Mg132 (Fig. 5**A and Supplement fig. 4B**). In B16F10 cell lines, inhibiting STING degradation efficiency peaked at 2-h chloroquine treatment (Fig. 5**B-C**). While in HCT116 cell lines, the effect of blocking STING degradation seemed to be most obvious after 1-h chloroquine (**Supplement fig. 4E-F**) or NH_4Cl (**Supplement fig. 4G-H**) treatment. To test whether the degradation was caused by STING monoubiquitination or polyubiquitination, we immunoprecipitated B16F10 cell line lysates with anti-STING antibody and validated ubiquitination levels (**Supplement fig. 4I**). It revealed that STING ubiquitination levels stayed the same in cell lines, suggesting that ubiquitination system did not play a role in STING degradation. To verify and visualize lysosomal colocalization of the STING protein, we immunostained for endogenous STING protein and lysosomal-associated membrane protein 1 (LAMP1) [27] in HCT116, HeLa, and 92.1 (Fig. 5**D and Supplement fig. 4J**) cells. It was observed that although STING protein expression was decreased in FBXO38-knockdown cells, the colocalization of STING protein with lysosomes was enhanced (Fig. 5**D**), indicating the efficacy of lysosomal degradation. Together, these data suggest that FBXO38-induced STING degradation was associated with lysosomal function.

Discussion

One important avenue to overcoming anti-PD1/PD-L1 resistance is to look for potential molecular mechanisms associated with anti-tumor immunity. FBXO38 is critical for PD-1 degradation and T cell immunity. However, how FBXO38 fully acts on the immune system has remained poorly understood. Here, we discovered that FBXO38 deficiency mediated lysosomal degradation of STING protein *in vivo* and *in vitro*, and further affected the activation of cGAS–STING pathway (Fig. 6). Although the involved molecular mechanism remains poorly understood, this work revealed a significant link between innate and adaptive immune pathways.

In previous studies, deficiencies in various genes have had different phenotypes in tumor cells and immune cells, and these have implications for targeted therapeutic measures. One example is the E3 ubiquitin ligase Casitas B lymphoma (c-Cbl). c-Cbl is another molecule that destabilizes PD-1 by ubiquitination-proteasomal degradation [28]. In tumor cells, c-Cbl exerts tumor suppressive effects by inhibiting Wnt/β-catenin as well as receptor and non-receptor tyrosine kinases [29,30]. An approach to activating c-Cbl was to use the c-Abl agonist DPH [31], which had been proven to restrict colitis. Another example is USP7, which belongs to the deubiquitinases (DUBs). A previous study showed that ectopic USP7 expression can suppress the poly-ubiquitination of FOXP3 protein to further decrease the suppressive capacity of regulatory T cells [32]. Another study showed that PD-L1 protein levels can be upregulated by inhibiting USP7 in Lewis tumor cells [33]. Additionally, an effective anti-tumor response was mobilized by combining USP7 inhibitor (P5091) with anti PD-1 therapy [33]. In summary, specific targets have been chosen to improve resistance to anti-PD1/PD-L1 therapy in recent studies. Our data show that FBXO38 can be as new molecular target for such therapeutic applications.

Ubiquitylation by the ubiquitin proteasome system is a type of PTM. E3 ligases are the most important enzymes for determining substrate specificity for ubiquitylation. SCF E3 ligase complexes are some of the best-characterized members of the E3 ligase family [34]. Currently, many studies had reported the effect of F-box proteins on tumor cells, such as FBXW7 [35], FBXO4 [36,37], and FBXO11 [38,39]. As a member of the SCF E3 ligase complexes, FBXO38 can participate in multiple cellular processes through ubiquitylation and subsequent proteasome degradation [40]. In the past, FBXO38 has been reported to mainly act through the ubiquitination proteasome pathway [19,20,22,41]. However, our study showed that FBXO38 deficiency mediated STING protein degradation through the lysosomal, rather than proteasomal pathway.

The mechanism is not explained in detail in this article. On one hand, there are few reports on lysosomal degradation of STING protein. It was reported that the half-life of STING was largely controlled by the lysosomal machinery, rather than by proteasomal degradation or autophagy [13,42]. At the end of the activation of the pathway, STING translocates to the lysosome, independently of TBK1 being phosphorylated, but depending by two conserved regions within the LBDα3 [13]. Additional studies are required to explore the underlying mechanism. On another hand, FBXO38 regulates proteins *via* the lysosomal pathway has not been reported. The literature describes other SCF family members that play functional roles through the lysosomal pathway. Deficiency in FBXL4 reduced steady-state levels of mitochondrial proteins. Because the phenotype could be reversed by lysosomal inhibition instead of proteasomal inhibition, the phenomenon was considered to be associated with autophagy [43]. Moreover, SCF^{FBXO27} can ubiquitinate glycoproteins in damaged lysosomes to initiate autophagy through the lysosomal protein LAMP2 [44]. In this regard, FBXO38 has the potential to regulate lysosomal degradation of STING by affecting lysosomal function. Future studies will probe the specific signals that assist FBXO38 in targeting STING for lysosomal degradation and clarify questions about related mechanisms.

In summary, we show that FBXO38-deficient tumor cells have increased growth *via* enhanced lysosomal degradation of STING protein. Importantly, the role of FBXO38 in both tumor and immune cells offers new insights into the crosstalk between adaptive and innate immune processes. Targeting this crosstalk in the tumor immune microenvironment could bear the promise of alleviating resistance to anti PD-1/PD-L1 therapy.

Funding

This work was supported by the General Program of the National Natural Science Foundation of China (No. 81972667 to J.S.), the National Key R&D Program of China (2021YFC2701103 to J.S.), the Shanghai Key Clinical Specialty, Shanghai Eye Disease Research Center (2022ZZ01003), and the Shanghai Municipal Education Commission-Two Hundred Talent (No. 20191817 to J.S.).

Author contributions

J.S., and X.F. provided direction and guidance throughout the preparation of this manuscript. Y.W. and Y.F. contributed equally to this

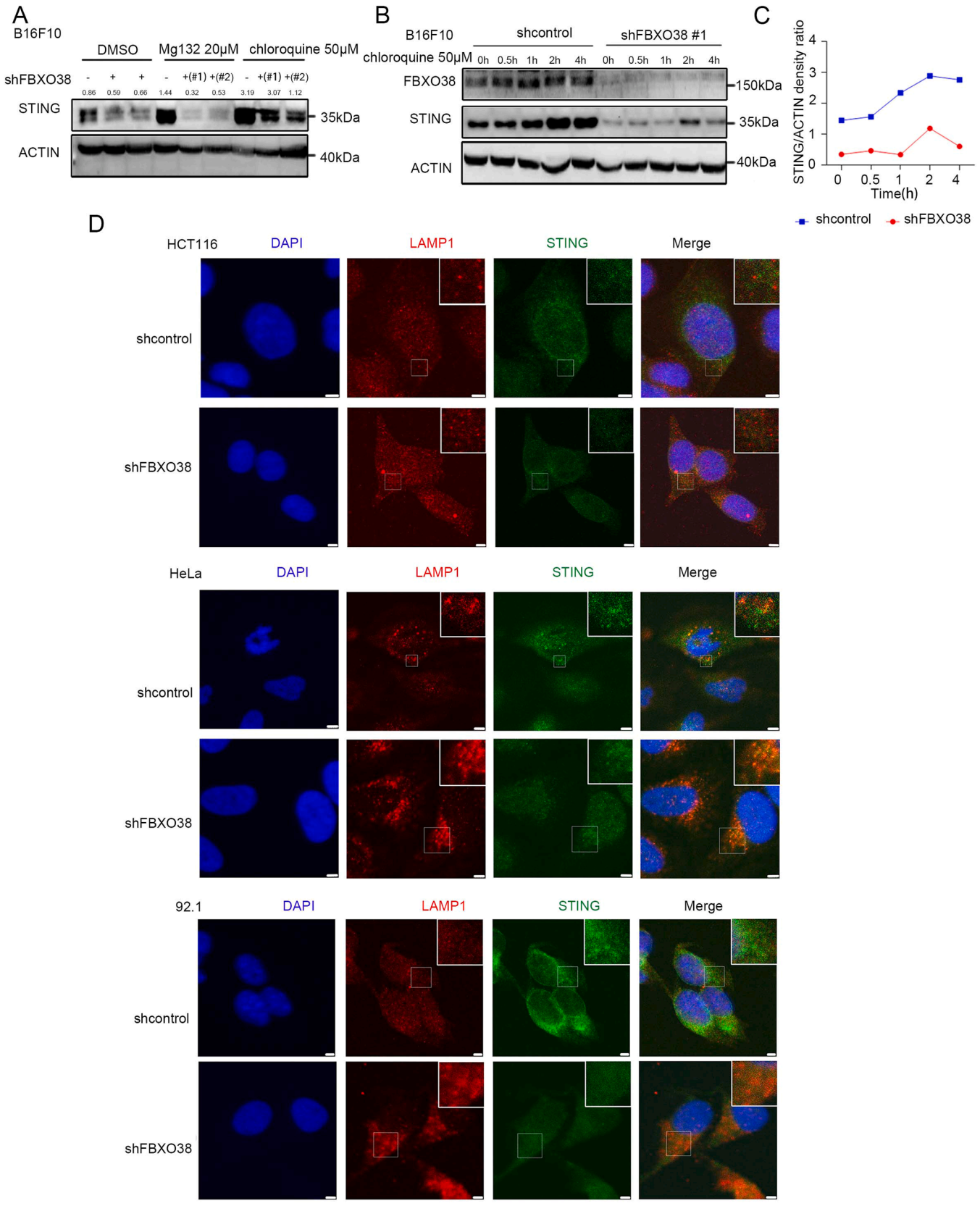

Fig. 5. FBXO38 mediated lysosome-depended STING degradation. A. Changes in the protein levels of FBXO38-knockdown B16F10 cells treated with DMSO, the proteasome inhibitor MG132 (20 μM), or the lysosome inhibitors chloroquine (50 μM) for 24h. **B-C.** FBXO38-knockdown B16F10 cells were treated with 50 μM chloroquine for different periods of time. FBXO38 and STING protein levels were monitored by immunoblotting. Protein decay analysis from **B** is shown in **C. D.** Immunofluorescence staining of STING (green) and the lysosomal marker LAMP1 (red) in control and FBXO38-knockdown cells, by confocal microscopy. Scale bars: 5 μm. The cells tested included HCT116, HeLa, and 92.1.

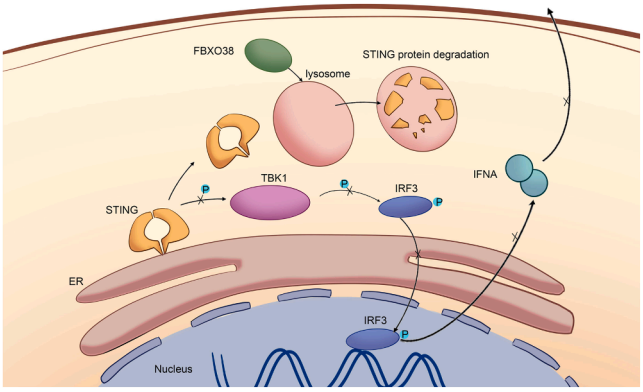

Fig. 6. Deficiency in FBXO38 led to lysosome-associated STING protein degradation.

manuscript. Y.W. and Y.F. collected and interpreted the study and were major contributors to the writing and editing of the manuscript. Y. L., R. H., F.S., Z.Z., and M.Z. made constructive revisions to the manuscript. All authors read and approved the final manuscript.

CRediT authorship contribution statement

Yijia Wu: Conceptualization, Data curation, Formal analysis, Investigation, Resources, Validation, Visualization, Writing – original draft, Writing – review & editing. **Yao Lin:** Data curation, Methodology, Supervision, Validation. **Feiyang Shen:** Investigation, Validation. **Rui Huang:** Investigation, Validation. **Zhe Zhang:** Methodology, Validation. **Min Zhou:** Supervision. **Yan Fang:** Conceptualization, Methodology, Supervision, Validation, Writing – review & editing. **Jianfeng Shen:** Conceptualization, Data curation, Formal analysis, Funding acquisition, Investigation, Methodology, Supervision, Validation. **Xianqun Fan:** Conceptualization, Data curation, Formal analysis, Funding acquisition, Resources, Supervision, Validation.

Declaration of competing interest

The authors declare that they have no known competing financial interests or personal relationships that could have appeared to influence the work reported in this paper.

Supplementary materials

Supplementary material associated with this article can be found, in the online version, at doi:10.1016/j.neo.2024.100973.

References

[1] M.A. Hossain, et al., Reinvigorating exhausted CD8+ cytotoxic T lymphocytes in the tumor microenvironment and current strategies in cancer immunotherapy, Med. Res. Rev. 41 (2021) 156–201.
[2] L. Zhu, J. Liu, J. Chen, Q. Zhou, The developing landscape of combinatorial therapies of immune checkpoint blockade with DNA damage repair inhibitors for the treatment of breast and ovarian cancers, J. Hematol. Oncol. 14 (2021) 206.
[3] Y. Wang, et al., cGAS-STING pathway in cancer biotherapy, Mol. Cancer 19 (2020) 136.
[4] H. Ishikawa, Z. Ma, G.N. Barber, STING regulates intracellular DNA-mediated, type I interferon-dependent innate immunity, Nature 461 (2009) 788–792.
[5] Y. Liu, et al., An inhalable nanoparticulate STING agonist synergizes with radiotherapy to confer long-term control of lung metastases, Nat. Commun. 10 (2019) 5108.
[6] O. Demaria, et al., STING activation of tumor endothelial cells initiates spontaneous and therapeutic antitumor immunity, Proc. Natl. Acad. Sci. U.S.A. 112 (2015) 15408–15413.
[7] D. Gao, et al., Cyclic GMP-AMP synthase is an innate immune sensor of HIV and other retroviruses, Science 341 (2013) 903–906.
[8] G. Shang, C. Zhang, Z.J. Chen, X.-C. Bai, X Zhang, Cryo-EM structures of STING reveal its mechanism of activation by cyclic GMP-AMP, Nature 567 (2019) 389–393.
[9] H. Ishikawa, G.N. Barber, STING is an endoplasmic reticulum adaptor that facilitates innate immune signalling, Nature 455 (2008) 674–678.
[10] S. Liu, et al., Phosphorylation of innate immune adaptor proteins MAVS, STING, and TRIF induces IRF3 activation, Science 347 (2015) aaa2630.
[11] W.M. Schneider, M.D. Chevillotte, C.M. Rice, Interferon-stimulated genes: a complex web of host defenses, Annu. Rev. Immunol. 32 (2014) 513–545.
[12] P. Hubel, et al., A protein-interaction network of interferon-stimulated genes extends the innate immune system landscape, Nat. Immunol. 20 (2019) 493–502.
[13] V.K. Gonugunta, et al., Trafficking-mediated STING degradation requires sorting to acidified endolysosomes and can be targeted to enhance anti-tumor response, Cell Rep. 21 (2017) 3234–3242.
[14] Q. Chen, L. Sun, Z.J. Chen, Regulation and function of the cGAS-STING pathway of cytosolic DNA sensing, Nat. Immunol. 17 (2016) 1142–1149.
[15] T. Saitoh, et al., Atg9a controls dsDNA-driven dynamic translocation of STING and the innate immune response, Proc. Natl. Acad. Sci. u S. a 106 (2009) 20842–20846.
[16] N. Dobbs, et al., STING activation by translocation from the ER is associated with infection and autoinflammatory disease, Cell Host. Microbe 18 (2015) 157–168.
[17] H. Konno, K. Konno, G.N. Barber, Cyclic dinucleotides trigger ULK1 (ATG1) phosphorylation of STING to prevent sustained innate immune signaling, Cell 155 (2013) 688–698.
[18] X. Hu, et al., Emerging role of ubiquitination in the regulation of PD-1/PD-L1 in cancer immunotherapy, Mol. Ther. 29 (2021) 908–919.
[19] X. Meng, et al., FBXO38 mediates PD-1 ubiquitination and regulates anti-tumour immunity of T cells, Nature 564 (2018) 130–135.
[20] S. Smaldone, F. Laub, C. Else, C. Dragomir, F. Ramirez, Identification of MoKA, a novel F-box protein that modulates Krüppel-like transcription factor 7 activity, Mol. Cell Biol. 24 (2004) 1058–1069.
[21] N. Dibus, et al., FBXO38 ubiquitin ligase controls sertoli cell maturation, Front. Cell Dev. Biol. 10 (2022) 914053.
[22] N. Dibus, V. Korinek, L. Cermak, FBXO38 ubiquitin ligase controls centromere integrity via ZXDA/B stability, Front. Cell *Dev. Biol.* 10 (2022) 929288.
[23] C.J. Sumner, et al., A dominant mutation in FBXO38 causes distal spinal muscular atrophy with calf predominance, Am. J. Hum. Genet. 93 (2013) 976–983.
[24] Z. Tang, et al., GEPIA: a web server for cancer and normal gene expression profiling and interactive analyses, Nucleic. Acids. Res. 45 (2017) W98–W102.
[25] Y. Zhu, et al., The combination of PD-1 blockade with interferon-α has a synergistic effect on hepatocellular carcinoma, Cell Mol. Immunol. 19 (2022) 726–737.
[26] T. Xia, X.-M. Yi, X. Wu, J. Shang, H.-B. Shu, PTPN1/2-mediated dephosphorylation of MITA/STING promotes its 20S proteasomal degradation and attenuates innate antiviral response, Proc. Natl. Acad. Sci. U.S.A. 116 (2019) 20063–20069.
[27] E.-L. Eskelinen, Roles of LAMP-1 and LAMP-2 in lysosome biogenesis and autophagy, Mol. Aspects. Med. 27 (2006) 495–502.
[28] C. Lyle, et al., c-Cbl targets PD-1 in immune cells for proteasomal degradation and modulates colorectal tumor growth, Sci. Rep. 9 (2019) 20257.
[29] M. Shashar, et al., c-Cbl mediates the degradation of tumorigenic nuclear β-catenin contributing to the heterogeneity in Wnt activity in colorectal tumors, Oncotarget. 7 (2016) 71136–71150.
[30] S. Shivanna, et al., The c-Cbl ubiquitin ligase regulates nuclear β-catenin and angiogenesis by its tyrosine phosphorylation mediated through the Wnt signaling pathway, J. Biol. Chem. 290 (2015) 12537–12546.
[31] J.-L. Duan, et al., E3 ligase c-Cbl regulates intestinal inflammation through suppressing fungi-induced noncanonical NF-κB activation, Sci. Adv. 7 (2021) eabe5171.
[32] J. van Loosdregt, et al., Stabilization of the transcription factor Foxp3 by the deubiquitinase USP7 increases Treg-cell-suppressive capacity, Immunity. 39 (2013) 259–271.
[33] X. Dai, et al., USP7 targeting modulates anti-tumor immune response by reprogramming tumor-associated macrophages in lung cancer, Theranostics. 10 (2020) 9332–9347.
[34] D. Frescas, M. Pagano, Deregulated proteolysis by the F-box proteins SKP2 and beta-TrCP: tipping the scales of cancer, Nat. Rev. Cancer 8 (2008) 438–449.
[35] K. Crusio, B. King, L. Reavie, I. Aifantis, The ubiquitous nature of cancer: the role of the SCFFbw7 complex in development and transformation, Oncogene 29 (2010) 4865–4873.
[36] E.K. Lee, et al., The FBXO4 tumor suppressor functions as a barrier to BRAFV600E-dependent metastatic melanoma, Mol. Cell Biol. 33 (2013) 4422–4433.
[37] Z. Lian, et al., FBXO4 loss facilitates carcinogen induced papilloma development in mice, Cancer Biol. Ther. 16 (2015) 750–755.
[38] K.M. Mann, et al., Sleeping Beauty mutagenesis reveals cooperating mutations and pathways in pancreatic adenocarcinoma, Proc. Natl. Acad. Sci. u S. a 109 (2012) 5934–5941.
[39] T. Abbas, et al., CRL1-FBXO11 promotes Cdt2 ubiquitylation and degradation and regulates Pr-Set7/Set8-mediated cellular migration, Mol. Cell 49 (2013) 1147–1158.
[40] Z. Wang, P. Liu, H. Inuzuka, W. Wei, Roles of F-box proteins in cancer, Nat. Rev. Cancer 14 (2014) 233–247.
[41] A. Georges, et al., USP7 Regulates Cytokinesis through FBXO38 and KIF20B, Sci. Rep. 9 (2019) 2724.
[42] X. Gui, et al., Autophagy induction via STING trafficking is a primordial function of the cGAS pathway, Nature 567 (2019) 262–266.
[43] D. Alsina, et al., FBXL4 deficiency increases mitochondrial removal by autophagy, EMBo Mol. Med. 12 (2020) e11659.
[44] Y. Yoshida, et al., Ubiquitination of exposed glycoproteins by SCFFBXO27 directs damaged lysosomes for autophagy, Proc. Natl. Acad. Sci. u S. a 114 (2017) 8574–8579.